Gate Current Calculations Using Spherical Harmonic Expansion of Boltzmann Equation

*Seonghoon Jin[1], Andreas Wettstein[2], Woosung Choi[1], Fabian M. Bufler[2,3], and Eugeny Lyumkis[1]

[1]Synopsys Inc. Mountain View, CA, US   [2]Synopsys Switzerland LLC Zürich, Switzerland

[3]Institut für Integrierte Systeme, ETH Zürich, Switzerland   *Email: sjin@synopsys.com

Abstract—A physics-based gate current model has been developed based on nonequilibrium electron energy distributions obtained from the spherical harmonic expansion of the Boltzmann equation. The model accounts for band structure effects, relevant microscopic scattering mechanisms, and electron injections caused by tunneling and thermionic emission processes with parallel momentum conservation and image potential barrier lowering. Obtained distribution functions and injection currents agree well with Monte Carlo simulations and experiments.

I. INTRODUCTION

Hot carrier injection into the gate oxide in MOSFETs is responsible for gate leakage and oxide degradation, and it has been used in the write operation in NOR flash memories. In order to model the hot carrier injection current, accurate knowledge of the nonequilibrium electron energy distribution is required. Although the Monte Carlo (MC) method would be the most rigorous tool to study hot electron transport [1], the MC method involves large statistical noise in the tail distribution that is important in the gate current calculation. This paper describes a gate current model based on the Spherical Harmonic Expansion (SHE) of the Boltzmann Transport Equation (BTE) [2], [3], [4], [5] that we have implemented in the device simulator Sentaurus Device [6]. The implemented SHE model accounts for the full band structure obtained from the empirical pseudopotential method (EPM) [7] and microscopic scattering mechanisms caused by acoustic and intervalley phonons, ionized impurities, and impact ionization. The implemented gate current model covers tunneling and thermionic emission components, and it takes into account parallel momentum conservation, image potential induced barrier lowering, and scattering probability within the image force potential well [1]. We validate our model by comparing obtained distribution functions and gate currents with MC simulations and experiments, and provide a gate current simulation example for a long-channel MOSFET where the hot electron injection is the dominant gate current mechanism.

II. DISTRIBUTION MODEL

In this work, electron energy distribution functions are obtained as a post-process with the conduction band energy E_C and the net recombination rate R_{net} given by drift-diffusion (DD) or hydrodynamic (HD) simulations. The lowest-order SHE of the BTE after the H-transformation reads [3]:

$$-\nabla \cdot \left[\frac{1}{3}\tau\left(\mathbf{r}, \varepsilon\right) g\left(\varepsilon\right) v^2\left(\varepsilon\right) \nabla f\left(\mathbf{r}, H\right)\right] = g\left(\varepsilon\right) s\left(\mathbf{r}, \varepsilon\right), \quad (1)$$

where $\mathbf{r}$ is the position, H is the total energy, $\varepsilon = H - E_C\left(\mathbf{r}\right)$ is the kinetic energy, v is the magnitude of the electron
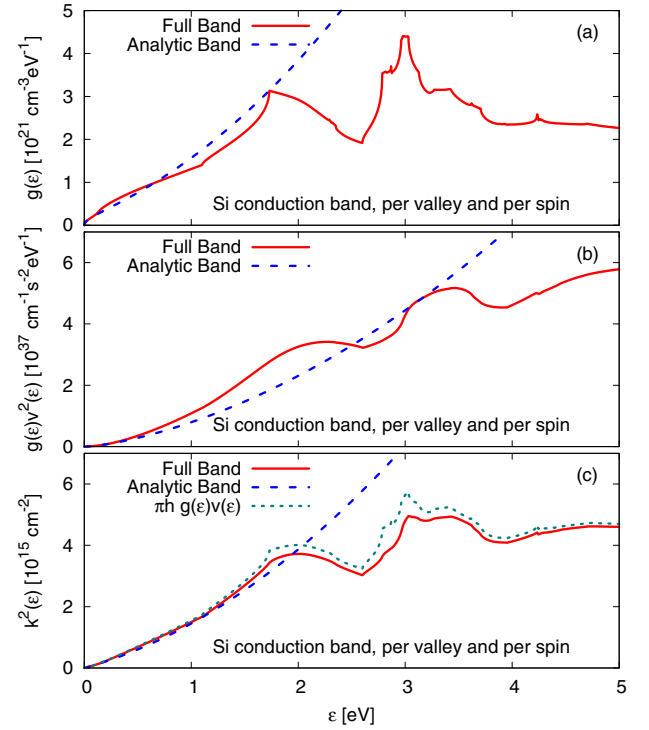

Fig. 1. Comparison of (a) $g\left(\varepsilon\right) \equiv \int_\varepsilon d\mathbf{s_k}/[8\pi^3\hbar\left|\mathbf{v}\left(\mathbf{k}\right)\right|]$, (b) $g\left(\varepsilon\right) v^2\left(\varepsilon\right) \equiv \int_\varepsilon d\mathbf{s_k}\left|\mathbf{v}\left(\mathbf{k}\right)\right|/(8\pi^3\hbar)$, and (c) $k^2\left(\varepsilon\right) \equiv \int_\varepsilon d\mathbf{s_k}/(4\pi)$ of the silicon conduction band obtained from the EPM bandstructure calculation and from the analytic band model. The integration $\int_\varepsilon d\mathbf{s_k}$ is over the equi-energy surface for a particular valley (the Brillouin zone is subdivided into six valleys [8]), including the sum over four conduction bands from the lowest one.

velocity, $1/\tau$ is the total scattering rate, g is the density-of-states, f is the occupation probability of electrons, and s is the net in-scattering rate due to inelastic scattering and generation-recombination processes. Equation (1) is a conservation equation with diffusion and source terms for a fixed total energy H, which can be discretized by the conventional box integration method with unstructured meshes. We obtain $g\left(\varepsilon\right)$, $g\left(\varepsilon\right) v^2\left(\varepsilon\right)$, and $k^2\left(\varepsilon\right)$ from the EPM bandstructure calculation [7] as shown in Fig. 1 where the dashed lines represent the results obtained from the analytic nonparabolic band model [9]: $g\left(\varepsilon\right) = 2\pi\left(2m_n\right)^{3/2}\sqrt{\varepsilon\left(1 + \alpha\varepsilon\right)}\left(1 + 2\alpha\varepsilon\right)/h^3$, $v^2\left(\varepsilon\right) = 2\varepsilon\left(1 + \alpha\varepsilon\right)/[m_c\left(1 + 2\alpha\varepsilon\right)^2]$, and $k^2\left(\varepsilon\right) = 2\pi^2\hbar g\left(\varepsilon\right) v\left(\varepsilon\right)$ with $m_n = 0.328\ m_0$, $m_c = 0.26\ m_0$, and $\alpha = 0.5$ /eV. Although the analytic band model works well for $\varepsilon < 1$ eV, it is important to use the full bandstructure for gate current calculations since the tail distribution is largely affected by the bandstructure for $\varepsilon > 1$ eV.

The total scattering rate and the net in-scattering rate can be written as:

$$\frac{1}{\tau} = \frac{1}{\tau_{\text{ac}}} + \frac{1}{\tau_{\text{ope}}} + \frac{1}{\tau_{\text{opa}}} + \frac{1}{\tau_{\text{c}}} + \frac{1}{\tau_{\text{ii}}}, \quad (2)$$

$$s(\varepsilon) = \frac{f(\varepsilon - \varepsilon_{\text{op}}) e^{-\frac{\varepsilon_{\text{op}}}{kT}} - f(\varepsilon)}{\tau_{\text{ope}}(\varepsilon)} + \frac{f(\varepsilon + \varepsilon_{\text{op}}) e^{\frac{\varepsilon_{\text{op}}}{kT}} - f(\varepsilon)}{\tau_{\text{opa}}(\varepsilon)} + \frac{f_{\text{loc}}(\varepsilon) - f(\varepsilon)}{\tau_{\text{ii}}(\varepsilon)} - \frac{R_{\text{net}} f_{\text{loc}}(\varepsilon)}{n}, \quad (3)$$

where $1/\tau_{\text{ac}}$, $1/\tau_{\text{ope}}$, $1/\tau_{\text{opa}}$, $1/\tau_{\text{c}}$, and $1/\tau_{\text{ii}}$ are scattering rates due to acoustic phonons, optical phonon emission, optical phonon absorption, Coulomb centers, and impact ionization, respectively, $\varepsilon_{\text{op}} = 60$ meV is the optical phonon energy, n is the electron density, R_{net} is the net recombination rate, and f_{loc} is the local equilibrium distribution function. The acoustic and optical phonon scattering rates can be written as [9]:

$$\frac{1}{\tau_{\text{ac}}(\varepsilon)} = \frac{2\pi k T D_{\text{ac}}^2}{\hbar \rho c_{\text{L}}^2} g(\varepsilon), \quad (4)$$

$$\frac{1}{\tau_{\text{ope}}(\varepsilon)} = \frac{\pi \hbar D_{\text{op}}^2}{\rho \varepsilon_{\text{op}}} (N_{\text{op}} + 1) g(\varepsilon - \varepsilon_{\text{op}}), \quad (5)$$

$$\frac{1}{\tau_{\text{opa}}(\varepsilon)} = \frac{\pi \hbar D_{\text{op}}^2}{\rho \varepsilon_{\text{op}}} N_{\text{op}} g(\varepsilon + \varepsilon_{\text{op}}), \quad (6)$$

where $D_{\text{ac}} = 9.27$ eV and $D_{\text{op}} = 1.25 \times 10^9$ eV/cm are the deformation potentials for acoustic and g-type optical phonons calibrated to reproduce the intrinsic bulk mobility, ρ is the mass density, c_{L} is the sound velocity, and N_{op} is the phonon number. The Coulomb scattering rate can be written as [8]:

$$\frac{1}{\tau_{\text{c}}(\varepsilon)} = \frac{q^4 \pi (N_{\text{D}} + N_{\text{A}}) g(\varepsilon) \zeta}{4 \hbar \epsilon_{\text{sem}}^2 k^4(\varepsilon)} \left[\ln(1+b) - \frac{b}{1+b} \right], \quad (7)$$

where $b = 4k^2(\varepsilon) k T \epsilon_{\text{sem}} / q^2 (n+p)$, ϵ_{sem} is the dielectric constant, and ζ is a fitting function introduced to match the Caughey-Thomas low-field mobility curve as a function of majority and minority doping concentrations. The impact ionization scattering rate can be written as [8]:

$$\frac{1}{\tau_{\text{ii}}(\varepsilon)} = \begin{cases} \left(\frac{\varepsilon - \varepsilon_{\text{ii},1}}{1 \text{ eV}} \right)^3 s_{\text{ii},1} & \varepsilon_{\text{ii},1} < \varepsilon < \varepsilon_{\text{ii},3} \\ \left(\frac{\varepsilon - \varepsilon_{\text{ii},2}}{1 \text{ eV}} \right)^2 s_{\text{ii},2} & \varepsilon > \varepsilon_{\text{ii},3} \end{cases}, \quad (8)$$

where $s_{\text{ii},1} = 1.49 \times 10^{11}$ s^{-1} and $s_{\text{ii},2} = 1.13 \times 10^{12}$ s^{-1} are the impact ionization coefficients, and $\varepsilon_{\text{ii},1} = 1.128$ eV, $\varepsilon_{\text{ii},2} = 1.572$ eV, and $\varepsilon_{\text{ii},3} = 1.75$ eV are the reference energies.

Figs. 2 and 3 compare the energy distribution functions obtained from the SHE and from the full-band MC method (Sentaurus MOCA and Sentaurus SPARTA [10]) for different uniform electric fields and for a 1D $n^+ - i - n^+$ structure with different drain voltages. The SHE method gives slightly smaller tail distribution compared with the MC method as we have intentionally used slightly large D_{op} in order to match the experimental gate current reported in [11].
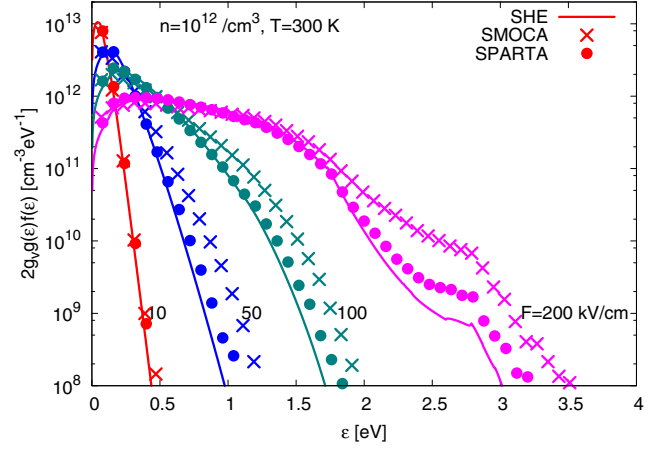

Fig. 2. Comparison of the electron energy distribution $[2g_v g(\varepsilon) f(\varepsilon)]$ obtained from the SHE method and from the full-band MC method (Sentaurus MOCA and Sentaurus SPARTA [10]) for different uniform electric fields ($F = 10$, 50, 100, and 200 kV/cm).
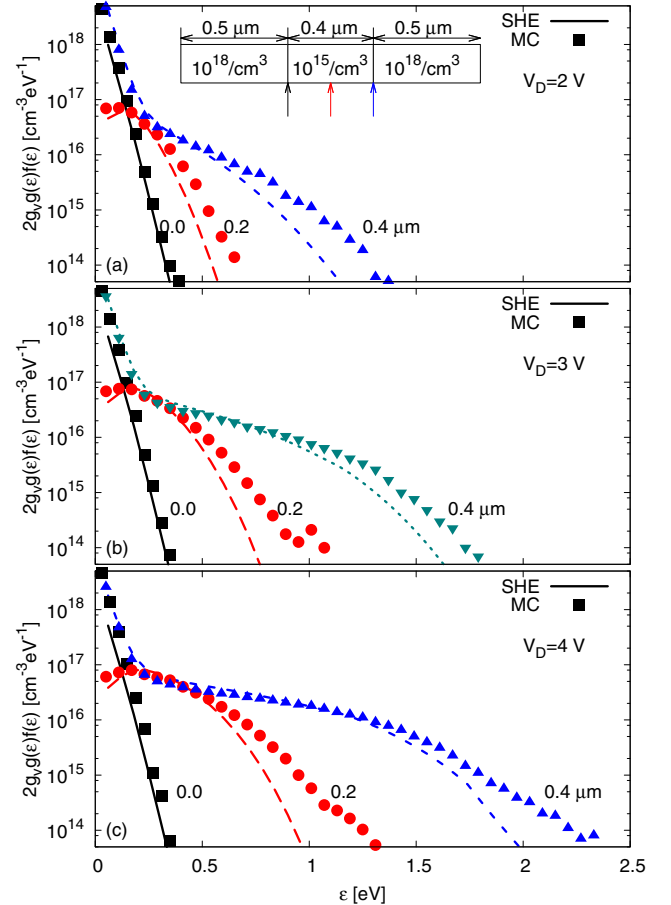

Fig. 3. Comparison of the electron energy distributions obtained from the SHE method and from the full-band MC method (Sentaurus MOCA) [10] for a 1D $n^+ - i - n^+$ structure with the channel length of 0.4 μm for (a) $V_{\text{D}} = 2$, (b) 3, and (c) 4 V. The potential profile obtained from the DD method is used in the SHE while the self-consistent potential is used in the MC method.

III. INJECTION MODEL

Once the electron energy distribution is available, the injection current density can be obtained from:

$$J_{\mathrm{g}} = 2qg_{\mathrm{v}}P_{\mathrm{ins}} \int_{\mathrm{v}} \frac{d\mathbf{k}}{(2\pi)^3} \left| \frac{\partial \varepsilon(\mathbf{k})}{2\hbar \partial k_\perp} \right| f[\varepsilon(\mathbf{k})] \Gamma[\varepsilon_{\mathrm{t}}(\mathbf{k})], \quad (9)$$

where $g_{\mathrm{v}} = 6$ is the valley degeneracy, $P_{\mathrm{ins}} = \exp(-r_0/\lambda_{\mathrm{ins}})$ is the probability of electrons moving from the interface to the barrier peak without scattering, r_0 is the distance from the interface to the barrier peak, $\lambda_{\mathrm{ins}} = 2$ nm is the mean free path in the insulator [1], $\Gamma(\varepsilon_{\mathrm{t}}) = \exp[-2\int_0^{t_{\mathrm{ins}}} \kappa(r, \varepsilon_{\mathrm{t}})\, dr]$ is the transmission coefficient obtained from the WKB approximation, and the integration $\int_{\mathrm{v}} d\mathbf{k}$ is over a particular valley and spin. The imaginary wavevector can be written as:

$$\kappa(r, \varepsilon_{\mathrm{t}}) = \hbar^{-1} \sqrt{2m_{\mathrm{ins}}[E_{\mathrm{B}}(r) - \varepsilon_{\mathrm{t}}]} \Theta[E_{\mathrm{B}}(r) - \varepsilon_{\mathrm{t}}], \quad (10)$$

$$E_{\mathrm{B}}(r) = E_{\mathrm{B}0} + qF_{\mathrm{ins}}r + E_{\mathrm{im}}(r), \quad (11)$$

$$E_{\mathrm{im}}(r) = -\frac{q^2}{16\pi\epsilon_{\mathrm{ins}}} \sum_{n=0}^{\infty} \tilde{\epsilon}^{2n+1} \left[\frac{1}{nt_{\mathrm{ins}} + r} + \frac{1}{(n+1)t_{\mathrm{ins}} - r} - \frac{2\tilde{\epsilon}}{(n+1)t_{\mathrm{ins}}} \right], \quad (12)$$

where $\epsilon_{\mathrm{ins}} = 2.15\,\epsilon_0$ is the high-frequency insulator dielectric constant [1], $\tilde{\epsilon} = (\epsilon_{\mathrm{sem}} - \epsilon_{\mathrm{ins}})/(\epsilon_{\mathrm{sem}} + \epsilon_{\mathrm{ins}})$, $m_{\mathrm{ins}} = 0.5\,m_0$ is the insulator effective mass [1], F_{ins} is the insulator electric field, $E_{\mathrm{B}0}$ is the barrier height, and Θ is the step function.

Taking into account the parallel momentum conservation during the tunneling process [1] and employing the spherical band approximation, we define the tunneling energy as follows:

$$\varepsilon_{\mathrm{t}}(\mathbf{k}) = \varepsilon(\mathbf{k}) - \frac{\hbar^2 k^2(\varepsilon)\sin^2\theta}{2m_{\mathrm{ins}}}, \quad (13)$$

where $k^2(\varepsilon) \approx 2\pi^2\hbar g(\varepsilon)v(\varepsilon)$ is the equi-energy surface area of the momentum space divided by 4π [see Fig. 1 (c)], and θ is the angle between $\mathbf{k}$ and the normal direction of the interface. Inserting (13) into (9) gives:

$$J_{\mathrm{g}} = P_{\mathrm{ins}} \int_0^{\infty} d\varepsilon j_\perp(\varepsilon) \int_0^1 dx\, \Gamma[\varepsilon - \gamma(\varepsilon)x], \quad (14)$$

where $j_\perp(\varepsilon) = 2qg_{\mathrm{v}}g(\varepsilon)v(\varepsilon)f(\varepsilon)/4$ and $\gamma(\varepsilon) = \pi^2\hbar^3 g(\varepsilon)v(\varepsilon)/m_{\mathrm{ins}}$. In the literature, there also exist different approximations of the tunneling energy: $\varepsilon_{\mathrm{t}}(\mathbf{k}) = \varepsilon$ (tunneling energy is equal to the kinetic energy [12], [13]) and $\varepsilon_{\mathrm{t}}(\mathbf{k}) = \varepsilon_\perp(\mathbf{k}) \approx \varepsilon(\mathbf{k})\cos^2\theta$ (tunneling energy is equal to the perpendicular component of the kinetic energy [14]). Within our SHE framework, these approximations give the following current density expressions:

$$J_{\mathrm{g}}^{(\varepsilon_{\mathrm{t}}=\varepsilon)} = P_{\mathrm{ins}} \int_0^{\infty} d\varepsilon j_\perp(\varepsilon) \Gamma(\varepsilon), \quad (15)$$

$$J_{\mathrm{g}}^{(\varepsilon_{\mathrm{t}}=\varepsilon_\perp)} = P_{\mathrm{ins}} \int_0^{\infty} d\varepsilon j_\perp(\varepsilon) \int_0^1 dx\, \Gamma(\varepsilon x). \quad (16)$$
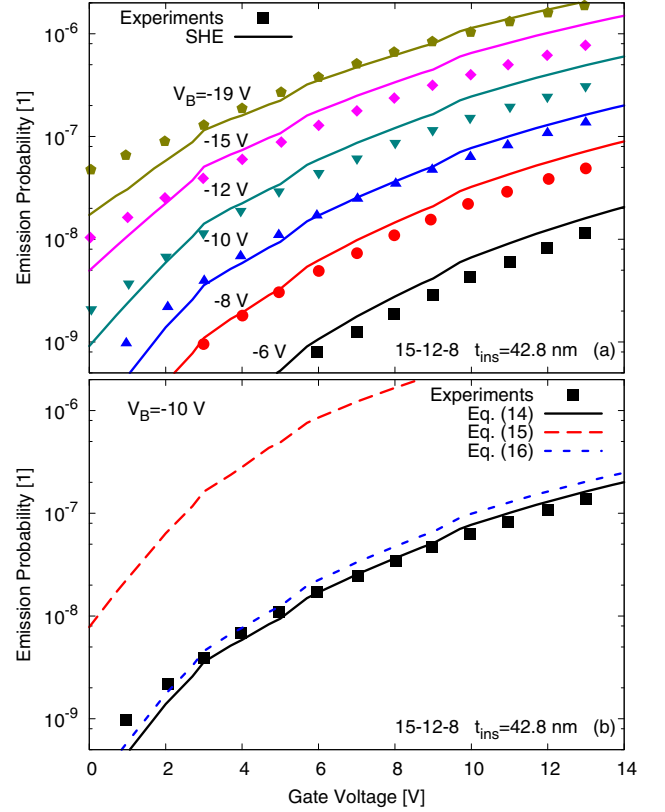

Fig. 4. Comparison of the emission probability of hot electrons obtained from measurements [11] and calculations.

In order to validate our injection model, we simulate the hot electron injection experiment reported in [11]. With a slight calibration of the barrier height ($E_{\mathrm{B}0} = 3.2$ instead of 3.1 eV), we can reproduce the experimental results quite well as shown in Fig. 4 (a). In Fig. 4 (b), we also compare (14) – (16) for the case of $V_{\mathrm{B}} = -10$ V. Equations (14) and (16) give very similar results while (15) gives too large emission probability.

IV. A LONG-CHANNEL MOSFET EXAMPLE

We study the gate current of a long-channel nMOSFET with $L_{\mathrm{eff}} = 0.8$ μm and $t_{\mathrm{ins}} = 21.5$ nm for different bias conditions as shown in Fig. 5. As the DD and HD models predict slightly different potential profiles and generation rates, the corresponding gate currents are different although the difference is relatively smaller than the difference observed in the lucky electron [15], [16] or Fiegna [12] model depending on the choice of the effective field. In order to see the influence of the impact ionization process, we have intentionally turned off the impact ionization process and compared the gate current in Fig. 5 (b). This shows that the impact ionization process significantly increases the gate current when a negative body voltage is applied as long as the gate voltage and drain voltage are relatively small. In Fig. 6, we plot the gate current density along the channel interface with and without
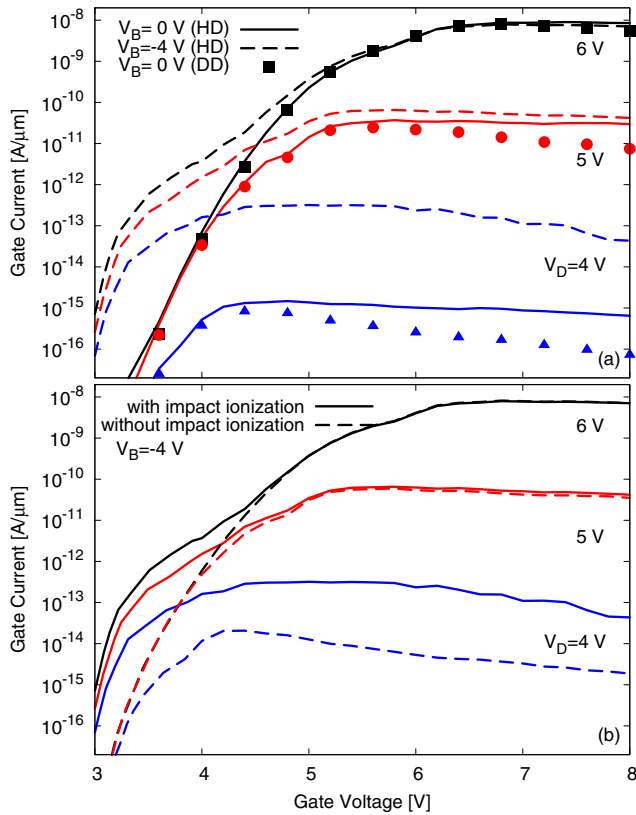
Fig. 5. Calculated gate current as a function of gate bias for a long channel nMOSFET with $L_{\text{eff}} = 0.8$ μm and $t_{\text{ox}} = 21.5$ nm.
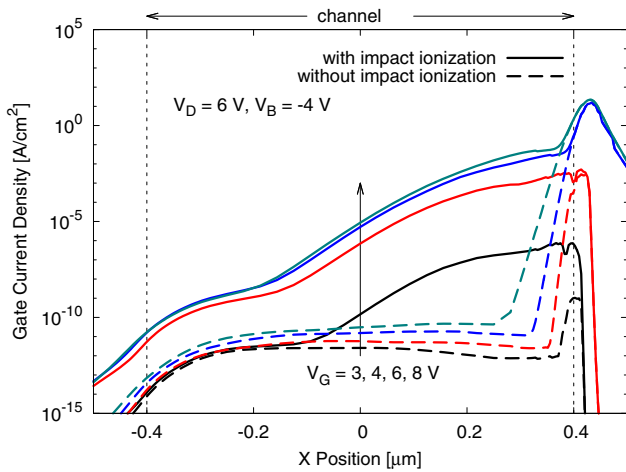

Fig. 6. Gate current density along the channel interface for different gate voltages when $V_D = 6$ V and $V_B = -4$ V, calculated with (solid lines) and without (dashed lines) the generation rate due to the impact ionization.

the impact ionization process, which shows that the impact ionization process increases gate current density in the middle of the channel by the channel-initiated secondary electron injection mechanism [17] while the gate current density at the drain end of the channel is determined by the channel hot electron injection [15].

V. CONCLUSION

We have implemented a gate current model based on the SHE of the BTE. The nonequilibrium energy distribution function obtained from the present model agrees well with the MC method, and the implemented injection model can reproduce the measured emission probability of hot electrons. We believe that this model will be useful for studying hot carrier injections in MOSFET devices and flash memories.

ACKNOWLEDGMENT

REFERENCES

[1] M. V. Fischetti, S. E. Laux, and E. Crabbé, "Understanding hot-electron transport in silicon devices: Is there a shortcut?" *Journal of Applied Physics*, vol. 78, no. 2, pp. 1058–1087, Jul. 1995.
[2] N. Goldsman, L. Henrickson, and J. Frey, "A physics-based analytical/numerical solution to the Boltzmann transport equation for use in device simulation," *Solid-state electronics*, vol. 34, no. 4, pp. 389–396, 1991.
[3] A. Gnudi, D. Ventura, G. Baccarani, and F. Odeh, "Two-dimensional MOSFET simulation by means of a multidimensional spherical harmonics expansion of the Boltzmann transport equation," *Solid-state electronics*, vol. 36, no. 4, pp. 575–581, 1993.
[4] S. Reggiani, M. C. Vecchi, and M. Rudan, "Investigation on electron and hole transport properties using the full-band spherical-harmonics expansion method," *IEEE Trans. Electron Devices*, vol. 45, no. 9, pp. 2010–2017, 1998.
[5] S. Hong, C. Jungemann, and M. Bollhöfer, "A deterministic Boltzmann equation solver for two-dimensional semiconductor devices," in *Intl. Conference on Simulation of Semiconductor Processes and Devices*, 2008, pp. 293–296.
[6] *Sentaurus Device User Guide*, Synopsys, Inc., Mountain View, CA, 2009. The support for the full band structure will be available in the Sentaurus Device version D-2010.03.
[7] M. M. Rieger and P. Vogl, "Electronic-band parameters in strained $Si_{1-x}Ge_x$ alloys on $Si_{1-y}Ge_y$ substrates," *Phys. Rev. B*, vol. 48, no. 19, pp. 14 276–14 287, 1993.
[8] C. Jungemann and B. Meinerzhagen, *Hierarchical Device Simulation: The Monte-Carlo Perspective*. Springer, 2003.
[9] C. Jacoboni and L. Reggiani, "The Monte Carlo method for the solution of charge transport in semiconductors with applications to covalent materials," *Rev. Mod. Phys.*, vol. 55, no. 3, pp. 645–705, Jul. 1983.
[10] *Sentaurus Device Monte Carlo User Guide*, Synopsys, Inc., Mountain View, CA, 2009.
[11] T. H. Ning, C. M. Osburn, and H. N. Yu, "Emission probability of hot electrons from silicon into silicon dioxide," *Journal of Applied Physics*, vol. 48, no. 1, pp. 286–293, Jan. 1977.
[12] C. Fiegna, F. Venturi, M. Melanotte, E. Sangiorgi, and B. Riccò, "Simple and efficient modeling of EPROM writing," *IEEE Trans. Electron Devices*, vol. 38, no. 3, pp. 603–610, Mar. 1991.
[13] A. Gehring, T. Grasser, H. Kosina, and S. Selberherr, "Simulation of hot-electron oxide tunneling current based on a non-Maxwellian electron energy distribution function," *Journal of Applied Physics*, vol. 92, no. 10, pp. 6019–6027, Nov. 2002.
[14] F. M. Bufler and A. Schenk, "On the Tunneling Energy within the Full-Band Structure Approach," in *Intl. Conference on Simulation of Semiconductor Processes and Devices*, 2005, pp. 155–158.
[15] S. Tam, P. K. Ko, and C. Hu, "Lucky-electron model of channel hot-electron injection in MOSFET'S," *IEEE Trans. Electron Devices*, vol. 31, no. 9, pp. 1116–1125, 1984.
[16] K. Hasnat, *et al.*, "A pseudo-lucky electron model for simulation of electron gate current in submicron NMOSFET's," *IEEE Trans. Electron Devices*, vol. 43, no. 8, pp. 1264–1273, 1996.
[17] J. D. Bude, A. Frommer, M. R. Pinto, and G. R. Weber, "EEPROM/flash sub 3.0 V drain-source bias hot carrier writing," in *International Electron Devices Meeting Tech. Digest*, 1995, pp. 989–992.